frontiers | Frontiers in Earth Science

TYPE Original Research
PUBLISHED 23 September 2022
DOI 10.3389/feart.2022.964055

OPEN ACCESS

EDITED BY
Wen Zhang,
Jilin University, China

REVIEWED BY
Yuanjun Jiang,
Chinese Academy of Sciences (CAS), China
Xiaoyi Fan,
Southwest Petroleum University, China

*CORRESPONDENCE
Binbin Zhao,
zhaobinbin@163.com

SPECIALTY SECTION
This article was submitted to Geohazards and Georisks, a section of the journal Frontiers in Earth Science

RECEIVED 08 June 2022
ACCEPTED 12 August 2022
PUBLISHED 23 September 2022

CITATION
Zhao B, Zhang Y, Liu Y, Kong X, Liu C, Xu X and Deng Y (2022), Calibration of effective interface friction angle in granular flow impact experiment. *Front. Earth Sci.* 10:964055. doi: 10.3389/feart.2022.964055

Calibration of effective interface friction angle in granular flow impact experiment

Binbin Zhao[1,2]*, Yingtian Zhang[3], Yi Liu[2], Xiaoang Kong[2], Chang Liu[2], Xiyu Xu[2] and Yuanjing Deng[2]

[1]Faculty of Engineering, China University of Geosciences, Wuhan, China, [2]China Electric Power Research Institute Co., Ltd, Beijing, China, [3]State Grid Smart Internet of Vehicles Co., Ltd, Beijing, China

By using the normal and tangential forces measured in experiments of granular flow impact against a retaining wall, the effective interface friction angle of the wall was calculated in the dynamic phase and the static phase respectively, designated as δ_{ec} and δ_{es}, and both of them are smaller than the interface friction angle measured by laboratory test (δ_2). It is found δ_{ec} shows an increasing trend against inclination angle (β), which is opposite to that of δ_{es}; and δ_{ec} has an underestimation of effective interface friction angle. By comparing the calculated normal forces of static phase and of dynamic phase with the measured values, it is found the lower bound relation between δ_{es}/δ_2 and β obtained from regression analysis could well calibrate the effective interface friction angle for both the wall and flume base. It is also noted that the increasing trend of δ_{ec} against β may be explained by the higher proportion of gravity-friction force at lower inclination angle, i.e., the higher proportion of drag force at higher inclination angle.

KEYWORDS

granular flow, interface friction angle, retaining wall, impact, calibration

1 Introduction

A granular flow impact, such as a landslide or a rock avalanche impinging against a retaining wall or other structures, could generate tremendous impact force on the structures against its flow (Sovilla et al., 2008; Faug et al., 2011). As concluded by Faug et al. (2009) and Jiang et al. (Jiang and Towhata., 2013; Jiang et al., 2015) in a granular flow impact event for both impact modes, see Figure 1, the force exerted on a retaining wall is basically composed of three force components: a drag force (F_d) (Buchholtz and Pöschel, 1998) and a passive earth force (F_p) (Savage and Hutter, 1989), both of them are produced by the flowing or inertial layer; and a gravity-and-friction induced force (F_{gf}) generated by the stagnant zone formed in front of the wall(Jiang and Towhata, 2013). According to the average velocity (v) and depth of flowing layer (h), and the weight of stagnant zone (G), the three force components could be calculated by the Eqs. 1–3.

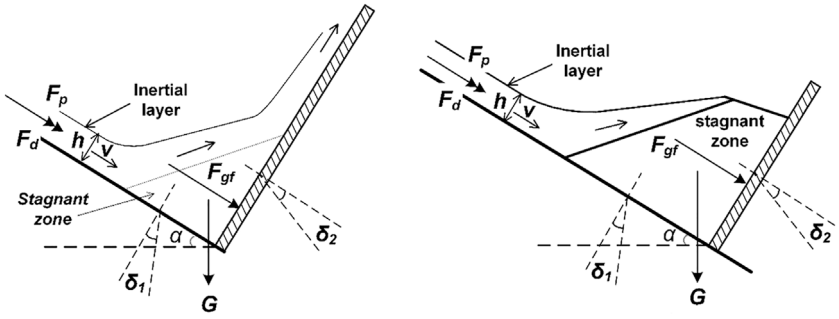

FIGURE 1
Drag force (F_d), passive earth force (F_p) and gravity-and-friction force (F_{gf}) respectively produced by inertial layer and stagnant zone in a granular flow impact event for two kinds of impact mode. δ_1 and δ_2 are respectively the interface friction angles of the flume base and the retaining wall.

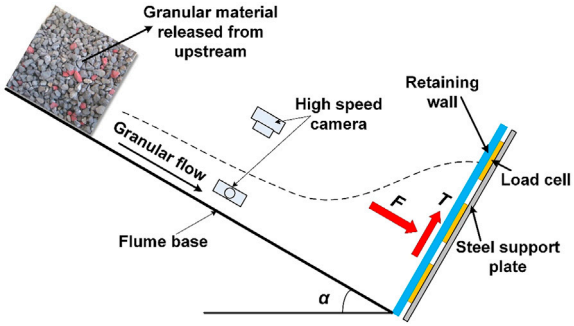

FIGURE 2
Experimental setup of granular material, flume and retaining wall model.

$$F_d = \frac{1}{2}\rho v^2 C_d h \tag{1}$$

In which $C_d = aFr^{-n} = a\left(\frac{v}{\sqrt{gh}}\right)^{-n}$

$$F_p = \frac{1}{2}k_p \rho g h^2 \cos\alpha \tag{2}$$

In which $k_p = \frac{\cos\alpha + \sqrt{\cos^2\alpha - \cos^2\varphi}}{\cos\alpha + \sqrt{\cos^2\alpha - \cos^2\varphi}}$

$$F_{gf} = G\frac{\sin(\alpha - \delta_1)}{\cos(\delta_1 + \delta_2)}\cos\delta_2 \tag{3}$$

In the previous research Bryant et al. (2014) reported that in a granular flow the actual basal friction is smaller than what measured in laboratory interface friction tests. While for a granular flow impact process Jiang et al. (2015) found for the stagnant zone the actual value of friction angle between granular material and the interface of retaining wall (δ_2 in Eq. 3) is also significantly smaller than the value measured by laboratory interface friction tests; also compared with δ_2, the reduction of δ_1.more significantly increases the value of F_{gf} calculated by Eq. 3. As a further extension of Jiang's previous work, this paper provides a more detailed study of the reduction of interface friction angle and a calibration of the effective interface friction angles for impact force calculation.

2 Experimental methodology

As shown in Figure 2, the height and width of the flume were 0.35 m, and 0.3 m, respectively. In order to simulate a granular flow impact process, a mass of limestone particles (named as *Particle1*) were released on the upstream of the flume with an inclination of α. There was a trigger gate in front face of the moving particles to control the release of the particles. After flowing a distance of 2.19 m, it impacted the retaining wall installed at the downstream of the flume. In the experiments the impact force exerted on the retaining wall was measured in both normal and tangential directions by an array of load cells. The total normal force (F) and total tangential force (T) could be deduced from the load cells records. The current methodology neglected the influence of non-uniform normal forces measured from the load cells and ignored the development of interface friction as a function of relative movement between the soil and the interface material. The motion of impact process and the surface velocity of granular flow were recorded by high speed cameras installed at the downstream of the flume. Each model test was named according to the length (L) and height (H) of the initial deposition, and the inclination angle of flume base (α), such as "*Particle1-L44-H20-α45*," which indicates an experiment of *Particle1* with an initial length and height of 44 and 20 cm, and a inclination angle of 45°. By changing initial length, height and inclination angle 64 tests were done in total.

By referring to Burkalow (1945), Pudasaini et al. (2007) and Jiang and Towhata (2013), the interface friction angles of *Particle1* with flume base, retaining wall and side wall were measured by laboratory tests. In the tests a paper cylinder with a diameter of more than 10 times of mean particle diameter (D_{50}) and a height of more than 5 times of D_{50}, was

TABLE 1 Physical properties of particle.

Property	Value
Minimum dry unit weight, γmin (kN/m3)	13.5
Maximum dry unit weight, γmax (kN/m3)	15.4
Mean particle diameter, D50 (mm)	14.1
Maximum particle diameter, Dmax (mm)	25.4
Minimum particle diameter, Dmin (mm)	1.68
Uniformity Coefficient, Cu	1.5
Dynamic internal friction angle, φ (°)	45
Basal friction angle, δ1 (°)	25
Friction angle of retaining wall, δ2 (°)	21
Friction angle of side wall, δ3(°)	15

friction. Then by slowly tilting the plate until the cylinder started to move, the inclination angle was recorded as the interface friction angle between *Particel1* and the plate. Physical properties of *Particle1* are listed in Table 1.

3 Results analysis

3.1 Reduction of interface friction

In order to calculate the effective interface friction angle in a granular flow impact process, first of all, the time history of the total normal force (F) and total tangential force (T) were plotted in Figure 3A. The force history could be categorized into two

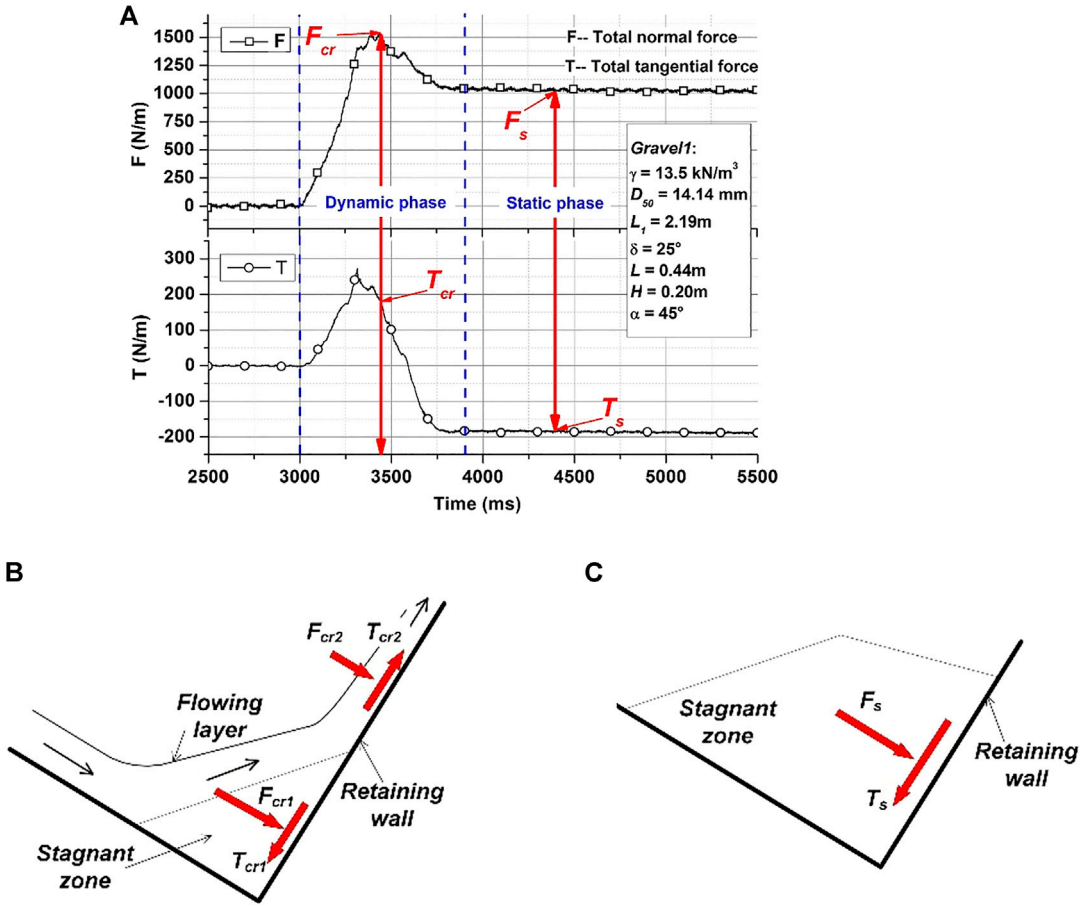

FIGURE 3
(A) Total normal and tangential forces history composed of dynamic and static phases, **(B)** Force generation mode in dynamic phase, **(C)** Force generation mode in static phase.

filled with *Particle1* and placed on the plate which is the same material as flume base or retaining wall or side wall. A gap of half D_{50} was kept between paper cylinder and the plate to avoid

phases: one is the dynamic phase, in which granular flow interacts with the retaining wall, both the flowing layer and the stagnant zone determine the force on the wall (Figure 3B); the

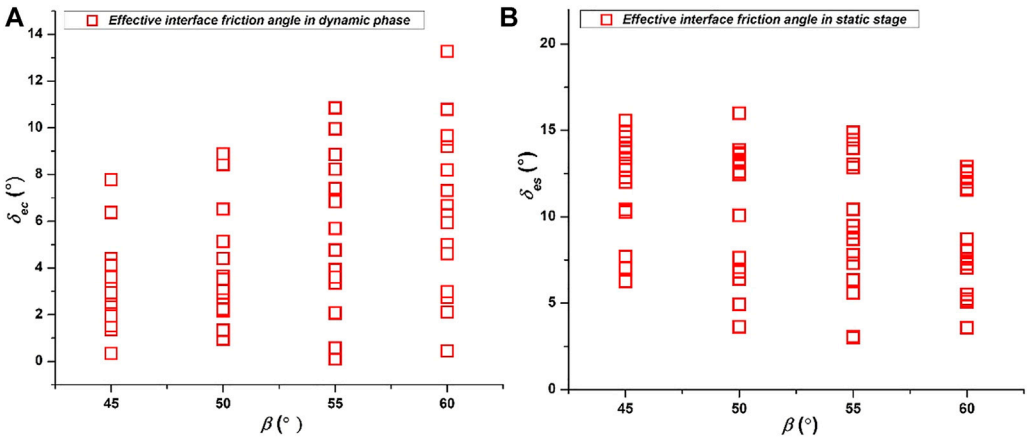

FIGURE 4
Variation of δ_{ec} and δ_{es} with interface inclination angle (β).

other is the static phase, in which granular flow ceases, only the stagnant zone generates force on the wall (Figure 3C). For the dynamic phase the forces were deduced at the time when maximum F occurred, and the corresponding normal and tangential forces are defined as F_{cr} and T_{cr}; while for the static phase, since both normal and tangential forces are constant, therefore, they were deduced at any time and defined as F_s and T_s.

F_{cr}, T_{cr}, F_s, and T_s were deduced for all the 64 experiments, thereafter, the effective interface friction angle of the dynamic phase was calculated by $\delta_{ec} = \arctan(|T_{cr}/F_{cr}|)$; and the effective interface friction angle of the static phase was calculated by $\delta_{es} = \arctan(|T_s/F_s|)$. In Figures 4A,B δ_{ec} and δ_{es} were respectively plotted against inclination angle of wall ($\beta = 90°-\alpha$) instead of inclination angle (α). In Figure 4A the maximum value of δ_{ec} is less than 14°, and in Figure 4B the maximum value of δ_{es} is less than 17°, which obviously indicates that both δ_{ec} and δ_{es} have a significant reduction from the laboratory measured δ_2 (21°). However, Figure 4A shows δ_{ec} increases with β, which is totally opposite to the decreasing trend of δ_{es} against β in Figure 4B. This divergence will be discussed in the last part of the paper.

As shown in Figure 3B in the dynamic phase the flowing layer produced a normal sub-force (F_{cr1}) and a tangential sub-force (T_{cr1}); meanwhile, the stagnant zone produce another pair of normal sub-force (F_{cr2}) and tangential sub-force (T_{cr2}). It is clear that the two tangential sub-forces are opposite in direction, which means the resultant tangential force is smaller than either T_{cr1} or T_{cr2}, i.e., the effective interface friction angle calculated from $\delta_{ec} = \arctan(|(T_{cr1} - T_{cr2})/(F_{cr1} + F_{cr2})|)$ is smaller than its actual value. While in Figure 3C there is only one tangential sub-force, i.e. the effective interface friction angle could be correctly calculated by $\delta_{es} = \arctan(|T_s/F_s|)$. Therefore, it is rational to assess the effective interface friction angle based on the normal and tangential forces in the static phase.

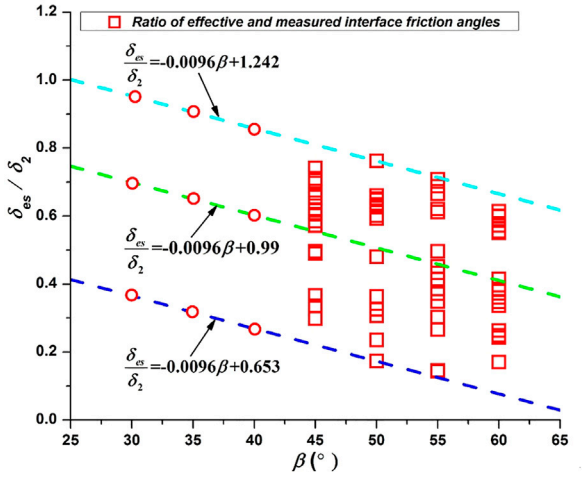

FIGURE 5
Relation of reduction rate of interface friction angle (δ_{es}/δ_2) and inclination angle (β); the red circle is where the value of δ_{es} will be calculated for flume base.

3.2 Calibration of effective interface friction angle

In Figure 4B the effective interface friction angle (δ_{es}) was calculated for the wall, however, from Figure 1 and Eq. 3 it is known that the normal force on the wall is determined by both the frictions of the wall and flume base. Therefore, it is also necessary to evaluate the effective interface friction angle of flume base. Since the laboratory measured interface friction angles of the wall and the flume base are close (Table 1), therefore, authors assume the reduction law for the wall and the flume base is the same; and if a relation between δ_{es} and β could be obtained from

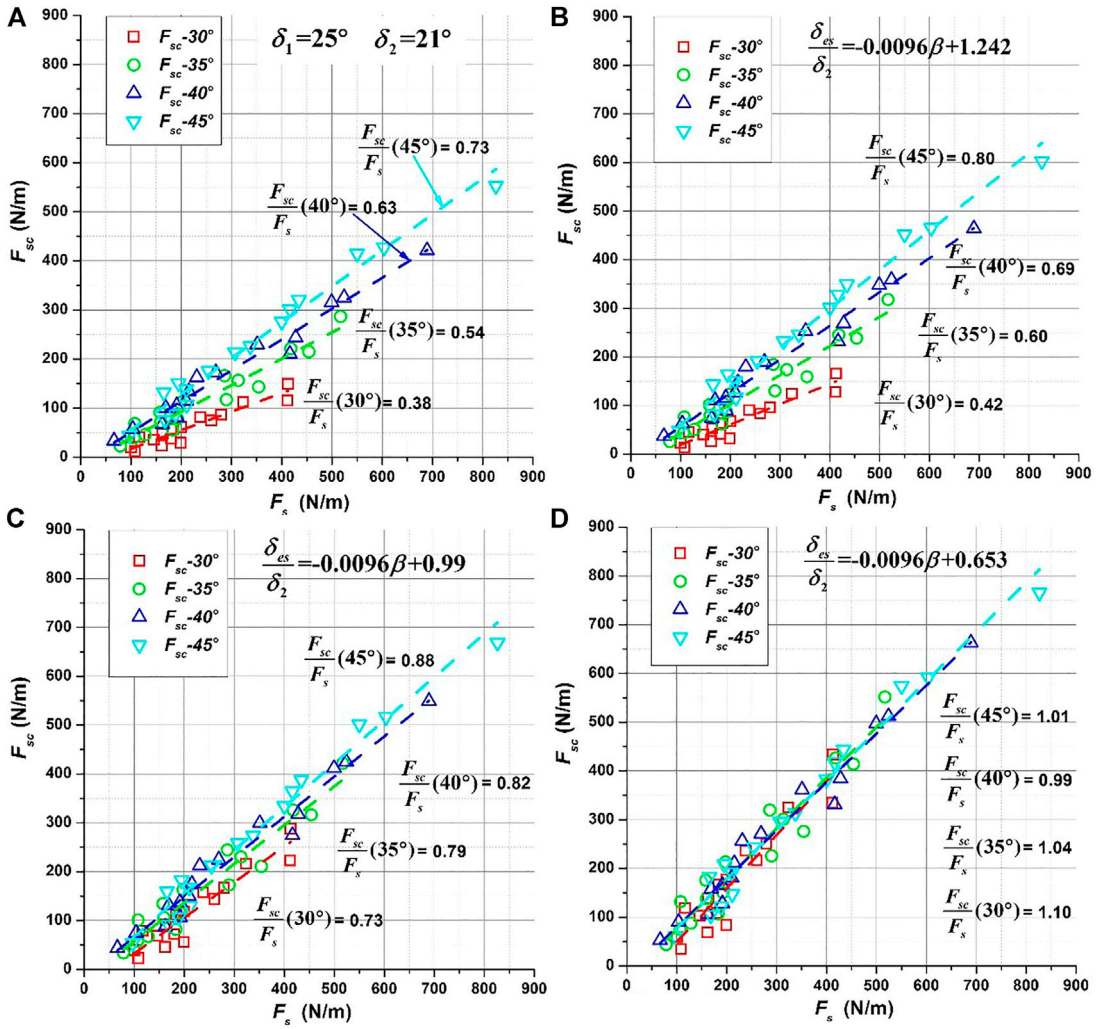

FIGURE 6
Comparison of calculated normal force of static phase (F_{sc}) with normal force of experimental measurement (F_s).

Figure 4B, it will be also applicable to the calibration of the effective interface friction angle of flume base.

In order to obtain one proper relation to calibrate δ_{es}, first, δ_{es} was normalized by δ_2 and plotted against β in Figure 5. The green dash line is the fitting of the data and defined as intermediate relation. Since for each β the value of δ_{es}/δ_2 has a wide scope, therefore, by offsetting the green line to the greatest and lowest bounds of δ_{es}/δ_2, an upper bound (light blue dash line) and a lower bound (deep blue dash line) relationships were found. According to the β of flume base and wall, the corresponding δ_{es} will be calculated. Consequently, it is going to be verified that if any of the relations could well calibrate δ_{es}.

In Figure 6, the normal force in static phase was calculated by Eq. 3 and designated as F_{sc}, and plotted against experimentally measured F_s. From Figures 6A–D the interface friction angles were either set as δ_1 and δ_2 or calculated by the three fitting relations in Figure 5.

Different colors was used to differentiate the results of different inclination angle. In Figure 6A it is clear that using δ_1 = 25° and δ_2 = 21° the calculated F_{sc} were smaller than the measured F_s; and with inclination angle (α) decreasing, the ratio of F_{sc} over F_s decreases from 0.73 to 0.38, i.e., the smaller the inclination angle is, the greater F_{sc} deviates from F_s.

From Figure 6B and Figure 6D, the ratio of F_{sc}/F_s get greater from upper bound relation to intermediate relation and to lower bound relation. As shown in Figure 6D for all the inclination angles the ratios of F_{sc}/F_s are close to 1.0, i.e., the lower bound relation gives the most accurate calibration of δ_{es}. As a second validation, the normal impact force of dynamic phase was calculated by summation of Eqs. 1,3 and designated as F_{sum}. In Figures 7A,B F_{sum} were respectively calculated by using the interface friction angle measured by laboratory test and that calibrated by lower bound relation, and were plotted

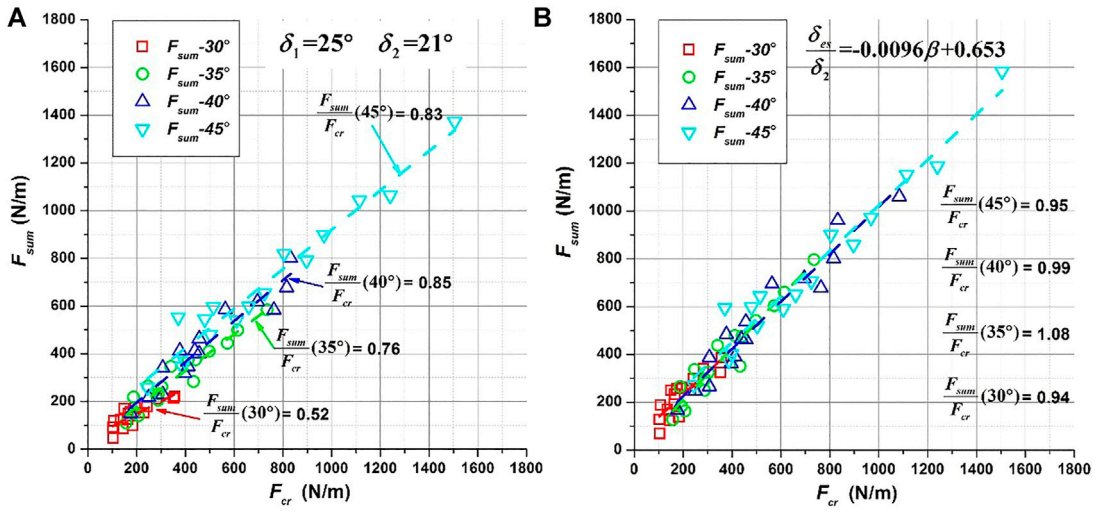

FIGURE 7
Comparison of calculated normal force of dynamic phase (F_{sum}) with normal force of experimental measurement (F_{cr}).

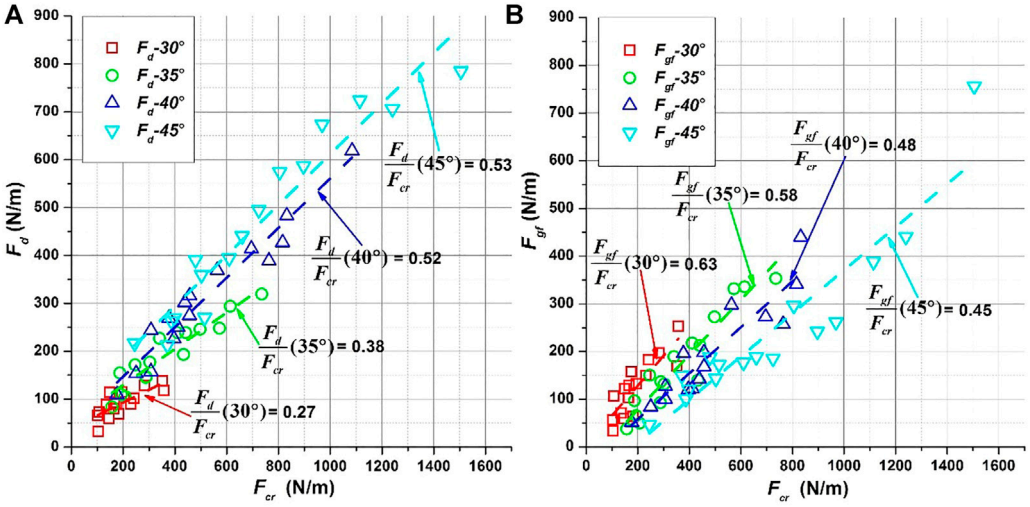

FIGURE 8
Dominant force component variation with inclination angle.

against the experimentally measured impact force (F_{cr}). In Figure 7A it is clear before calibration the ratio of F_{sum}/F_{cr} is always smaller than 1.0, and also decreases with inclination angle; for inclination angle of 30° the F_{sum} is only half of F_{cr}. After calibration for all the inclination angles the ratio of F_{sum}/F_{cr} is very close to 1.0, which once again indicates that the lower bound relation is suitable for the calibration of effective interface friction angle.

4 Discussion

In Section 3, Figures 4A,B present two opposite trends between δ_{es} and β. Since Figure 4B is already validated to be the correct representation of effective interface friction angle, hereby, the reason for the decreasing trend between δ_{ec} and β in Figure 4A is going to be discussed. First, the two main force components, F_d and F_{gf}, were respectively plotted against F_{cr}

in Figure 8, in which Figure 8A shows for higher inclination angle the proportion of F_d is higher; and Figure 8B shows for lower inclination angle the proportion of F_{gf} is higher. For higher inclination angle where the drag force is in domination (Figure 8A), the relatively thicker flowing layer (Figure 1A) produces more upward tangential sub-force; vice versa, for lower inclination angle where the gravity-and-friction force is dominating (Figure 8B), the flowing layer is thinner (Figure 1B), and less upward tangential sub-force is produced. Consequently, for higher inclination angle the resultant tangential force is relatively smaller, the effective friction angle calculated by $\delta_{ec} = \arctan(|(T_{cr1} - T_{cr2})/(F_{cr1} + F_{cr2})|)$ is accordingly smaller, which accounts for the trend in Figure 4A.

5 Conclusion

The effective interface friction angle of the wall calculated for the dynamic phase and the static phase (δ_{ec} and δ_{es}) are smaller than the laboratory measured δ_2. It is found δ_{ec} shows an increasing trend against inclination angle (β), which is opposite to that of δ_{es}; and δ_{ec} has an underestimation of effective interface friction angle. By using regression analysis an upper bound relation, an intermediate relation and a lower bound relation were obtained for δ_{es}/δ_2 and β. It is found the lower bound relation could well calibrate the effective interface friction angle for both the wall and flume base. It is also noted that the increasing trend of δ_{ec} against β in Figure 4A may be explained by the higher proportion of gravity-friction force at lower inclination angle, i.e., the higher proportion of drag force at higher inclination angle.

Data availability statement

The raw data supporting the conclusion of this article will be made available by the authors, without undue reservation.

Author contributions

BZ contributed to conception and investigation of the study and wrote the first draft of the manuscript. All authors contributed to manuscript revision, read, and approved the submitted version.

Funding

This study was funded by the National Key R&D Program of China, grant number 2018YFC0809400.

Conflict of interest

Authors BZ, YL, XK, CL, XX and YD were employed by China Electric Power Research Institute Co., Ltd. Author YZ was employed by State Grid Smart Internet of Vehicles Co., Ltd.

Publisher's note

References

Bryant, S. K., Take, W. A., and Bowman, E. T. (2014). Observations of grain-scale interactions and simulation of dry granular flows in a large-scale flume. *Can. Geotech. J.* 52, 638–655. Published on the web 19 September 2014. doi:10.1139/cgj-2013-0425

Buchholtz, V., and Pöschel, T. (1998). Interaction of a granular stream with an obstacle. *Granul. Matter* 1, 33–41. doi:10.1007/pl00010908

Burkalow, A. (1945). Angle of repose and angle of sliding friction: An experimental study. *Geol. Soc. Am. Bull.* 56 (6), 669–707. doi:10.1130/0016-7606(1945)56[669:aoraao]2.0.co;2

Faug, T., Beguin, R., and Chanut, B. (2009). Mean steady granular force on a wall overflowed by free-surface gravity-driven dense flows. *Phys. Rev. E* 80, 021305. doi:10.1103/physreve.80.021305

Faug, T., Caccamo, P., and Chanut, B. (2011). Equation for the force experienced by a wall overflowed by a granular avalanche: Experimental verification. *Phys. Rev. E* 84, 051301. doi:10.1103/physreve.84.051301

Jiang, Y.-J., and Towhata, I. (2013). Experimental study of dry granular flow and impact behavior against a rigid retaining wall. *Rock Mech. Rock Eng.* 46 (4), 713–729. doi:10.1007/s00603-012-0293-3

Jiang, Y. J., Zhao, Y., Towhata, I., and Liu, D.-X. (2015). Influence of particle characteristics on impact event of dry granular flow. *Powder Technol.* 270, 53–67. doi:10.1016/j.powtec.2014.10.005

Pudasaini, S. P., Hutter, K., Hsiau, S-S., Tai, S-C., Wang, Y., and Katzenbach, R. (2007). Rapid flow of dry granular materials down inclined chutes impinging on rigid walls. *Phys. Fluids (1994).* 19 (5), 053302. doi:10.1063/1.2726885

Savage, S. B., and Hutter, K. (1989). The motion of a finite mass of granular material down a rough incline. *J. Fluid Mech.* 199, 177–215. doi:10.1017/s0022112089000340

Sovilla, B., Schaer, M., Kern, M., and Bartelt, P. (2008). Impact pressures and flow regimes in dense snow avalanches observed at the vallée de la sionne test site. *J. Geophys. Res.* 113 (F1), F01010.

Glossary

a Empirical constant

T Total tangential force, N/m

g Gravitational acceleration, m/s^{-2}

T_{cr} Total tangential forces of dynamic phase, N/m

h Flow thickness, m

T_{cr1} Tangential sub-force of dynamic phase, N/m

k_p Passive earth pressure coefficient

T_{cr2} Tangential sub-force of dynamic phase, N/m

n Empirical constant

T_s Total tangential force of static phase, N/m

v Depth-averaged velocity, m/s

D_{min} Minimum particle diameter, mm

C_d Empirical drag coefficient

α Inclination angle of flume base, °

D_{50} Mean particle diameter, mm

β Inclination angle, °

D_{max} Maximum particle diameter, m

γ_{min} Minimum dry unit weight, kN/m^3

Fr Froude number

γ_{max} Maximum dry unit weight, kN/m^3

F Total normal force, N/m

δ_1 Interface basal friction angle, °

F_{cr} Total normal force of dynamic phase, N/m

δ_2 Interface friction angle of retaining wall, °

F_{cr1} Normal sub-force of dynamic phase, N/m

δ_3 Interface friction angle of side wall, °

F_{cr2} Normal sub-force of dynamic phase, N/m

δ_{ec} Equivalent interface friction angle of dynamic phase, °

F_s Total normal force of static phase, N/m

δ_{es} Equivalent interface friction angle of static phase, °

F_{sum} Total normal force calculated by equation, N/m

θ Angle of repose, °

G Weight of the stagnant zone, N/m

ρ Density of granular flow, kN/m^3

H Height of the initial deposit, m

φ Dynamic internal friction angle, °

L Length of the initial deposit, m

Fd Drag force, N/m

Fp, Passive earth force, N/m

Fgf Gravity-and-friction-induced force, N/m

Kp Passive coefficient